Monthly Notices
of the
ROYAL ASTRONOMICAL SOCIETY

Mon. Not. R. Astron. Soc. **415,** 1647–1662 (2011) doi:10.1111/j.1365-2966.2011.18800.x

Galaxy and Mass Assembly (GAMA): the star formation rate dependence of the stellar initial mass function

M. L. P. Gunawardhana,[1,2,3⋆] A. M. Hopkins,[2⋆] R. G. Sharp,[2] S. Brough,[2] E. Taylor,[3] J. Bland-Hawthorn,[3] C. Maraston,[4] R. J. Tuffs,[5] C. C. Popescu,[6] D. Wijesinghe,[3] D. H. Jones,[2,7] S. Croom,[3] E. Sadler,[3] S. Wilkins,[8] S. P. Driver,[9] J. Liske,[10] P. Norberg,[11] I. K. Baldry,[12] S. P. Bamford,[13] J. Loveday,[14] J. A. Peacock,[11] A. S. G. Robotham,[9] D. B. Zucker,[1,2] Q. A. Parker,[1,2] C. J. Conselice,[13] E. Cameron,[9,15] C. S. Frenk,[16] D. T. Hill,[9] L. S. Kelvin,[9] K. Kuijken,[17] B. F. Madore,[18] B. Nichol,[5] H. R. Parkinson,[11] K. A. Pimbblet,[7] M. Prescott,[12] W. J. Sutherland,[19] D. Thomas[5] and E. van Kampen[10]

[1]*Department of Physics and Astronomy, Macquarie University, Sydney, NSW 2109, Australia*
[2]*Australian Astronomical Observatory, Epping, NSW 1710, Australia*
[3]*Sydney Institute for Astronomy, School of Physics, University of Sydney, NSW 2006, Australia*
[4]*Institute of Cosmology and Gravitation (ICG), University of Portsmouth, Dennis Sciama Building, Burnaby Road, Portsmouth PO1 3FX*
[5]*Max Planck Institute for Nuclear Physics (MPIK), Saupfercheckweg 1, D-69117 Heidelberg, Germany*
[6]*Jeremiah Horrocks Institute, University of Central Lancashire, Preston PR1 2HE*
[7]*School of Physics, Monash University, Clayton, Victoria 3800, Australia*
[8]*Department of Physics, University of Oxford, Denys Wilkinson Building, Keble Road, Oxford OX1 3RH*
[9]*Scottish Universities Physics Alliance (SUPA), School of Physics and Astronomy, University of St Andrews, North Haugh, St Andrews, Fife KY16 9SS*
[10]*European Southern Observatory, Karl-Schwarzschild-Str. 2, 85748 Garching, Germany*
[11]*Scottish Universities Physics Alliance, Institute for Astronomy, University of Edinburgh, Royal Observatory, Blackford Hill, Edinburgh EH9 3HJ*
[12]*Astrophysics Research Institute, Liverpool John Moores University, Twelve Quays House, Egerton Wharf, Birkenhead CH41 1LD*
[13]*Centre for Astronomy and Particle Theory, University of Nottingham, University Park, Nottingham NG7 2RD*
[14]*Astronomy Centre, University of Sussex, Falmer, Brighton BN1 9QH*
[15]*Department of Physics, Swiss Federal Institute of Technology (ETH-Zürich), CH-8093 Zürich, Switzerland*
[16]*Institute for Computational Cosmology, Department of Physics, Durham University, South Road, Durham DH1 3LE*
[17]*Leiden University, PO Box 9500, NL-2300 RA Leiden, the Netherlands*
[18]*Observatories of the Carnegie Institution for Science, 813 Santa Barbara Street, CA 91101, USA*
[19]*Astronomy Unit, Queen Mary University London, Mile End Rd, London E14NS*

Accepted 2011 March 28. Received 2011 March 7; in original form 2010 July 31

ABSTRACT

The stellar initial mass function (IMF) describes the distribution in stellar masses produced from a burst of star formation. For more than 50 yr, the implicit assumption underpinning most areas of research involving the IMF has been that it is universal, regardless of time and environment. We measure the high-mass IMF slope for a sample of low-to-moderate redshift galaxies from the Galaxy and Mass Assembly survey. The large range in luminosities and galaxy masses of the sample permits the exploration of underlying IMF dependencies. A strong IMF–star formation rate dependency is discovered, which shows that highly star-forming galaxies form proportionally more massive stars (they have IMFs with flatter power-law slopes) than galaxies with low star formation rates. This has a significant impact on a wide variety of galaxy evolution studies, all of which rely on assumptions about the slope of the IMF. Our result is supported by, and provides an explanation for, the results of numerous recent explorations suggesting a variation of or evolution in the IMF.

Key words: galaxies: evolution – galaxies: formation – galaxies: star formation – galaxies: stellar content.

1 INTRODUCTION

The stellar initial mass function (IMF) is an empirical power-law relation describing the distribution of stellar masses formed in a

⋆E-mail: mlpg@physics.usyd.edu.au (MLPG); ahopkins@aao.gov.au (AMH)

single episode of star formation. This initial stellar mass distribution has often been assumed to be universal. This is perhaps the most fundamental assumption used in all galaxy formation and evolution studies. The IMF is the bridge between the massive stars, measurable through tracers such as Hα, ultraviolet, far-infrared and radio luminosity, and the low mass stars, which form the bulk of the stellar mass in galaxies (Kennicutt 1998). The IMF is intimately involved in many aspects of the modelling of galaxy evolution. Some examples include models of turbulent fragmentation and collapse of gas clouds that form sub-stellar to super-stellar objects (Nakamura & Umemura 2001), the numerical study of supersonic hydrodynamics and magnetohydrodynamics of turbulence (Padoan et al. 2007), gradual processes behind building of a galaxy (Gibson & Matteucci 1997), the reionization of the intergalactic medium at high redshift ($z > 6$) (Chary 2008), the relationship between stellar mass and star formation rate (SFR) (Davé 2008), evolution in colour and mass-to-light ratio of galaxies (van Dokkum 2008), models of heavy element production, chemical enrichment and evolution in galaxies (Calura & Menci 2009) from the death of stars, the fraction of stars that form black holes (Fryer 2003) and many other evolutionary processes.

The IMF is often parametrized as one or more power laws, describing the number of stars within a given mass interval, $\frac{\mathrm{d}N}{\mathrm{d}M} \propto m^{\alpha}$ with α defining the slope for the mass range of interest (Salpeter 1955; Baldry & Glazebrook 2003). Other widely adopted functional forms for the IMF include a lognormal form for the low-mass regime with a power-law tail for high masses (Chabrier 2001). From star counts of local resolved stellar populations, the IMF is measured to have a high-mass ($m > 0.5\,\mathrm{M}_{\odot}$) slope of $\alpha \approx -2.35$ (Salpeter 1955; Scalo 1986), also called the Salpeter slope, although variations of this slope are also reported (Miller & Scalo 1979; Kroupa, Tout & Gilmore 1993; Kroupa 2001). An 'integrated galaxy' IMF (IGIMF) has recently been proposed for the interpretation of the galaxy-wide IMF properties. Whether the IGIMF is universal (Elmegreen 2006) or differs from the star cluster IMF (Weidner & Kroupa 2005, 2006) is again a much debated subject. The dependence of cluster formation on the SFR of a galaxy is argued to give rise to a varying IGIMF (Weidner & Kroupa 2005), although the underlying IMF may still be universal. In almost all cases, the high-mass IMF slope is modelled with a power-law-type behaviour and a multi-part IMF expression best describes the stellar luminosity function in the solar neighbourhood (Scalo 1986; Kroupa et al. 1993). Therefore, a multi-part power law is used to obtain the results presented here. For the purpose of this investigation, we primarily use a two-part power law with a Salpeter high-mass ($>0.5\,\mathrm{M}_{\odot}$) slope and $\alpha = -1.3$ low-mass ($0.1 \leq M/\mathrm{M}_{\odot} \leq 0.5$) slope. The use of other popular functional forms of the IMF (Miller & Scalo 1979; Scalo 1986; Kroupa 2001) do not influence the overall conclusions of this study.

Turbulent star-forming gas and clump mass functions (Reid & Wilson 2005) indicate that a Salpeter-like IMF slope may be imprinted on the mass distribution of turbulent structures, and that all stellar clusters formed out of these structures therefore inherit a Salpeter-like IMF. The concept of a 'universal IMF' is, however, being increasingly scrutinized by recent studies based on large samples of galaxies and non-traditional approaches, all reporting discrepancies between the observations and model predictions. A number of recent studies now suggest an evolving or spatially varying IMF as a 'last resort' explanation to reconcile the observed differences (Hoversten & Glazebrook 2008; Wilkins, Trentham & Hopkins 2008b; Wilkins et al. 2008a; van Dokkum 2008; Meurer et al. 2009). The assumed cosmological parameters are: $H_0 = 70\,\mathrm{km\,s^{-1}\,Mpc^{-1}}$, $\Omega_{\mathrm{M}} = 0.3$ and $\Omega_{\wedge} = 0.7$.

2 OBSERVATIONS

2.1 Galaxy and Mass Assembly survey

Motivated by these recent failures of the universal IMF assumption, we have conducted an analysis exploring such variations using a sample of galaxies from the Galaxy and Mass Assembly (GAMA) survey (Driver et al. 2009; Robotham et al. 2009; Baldry et al. 2009). GAMA is a spectroscopic survey with multi-wavelength photometric data undertaken at the Anglo-Australian Telescope using the 2dF fibre feed and AAOmega multi-object spectrograph. AAOmega provides 5 Å resolution spectra with complete spectral coverage from 3700 to 8800 Å (Sharp et al. 2006). GAMA covers three equatorial fields of 48 deg^2 each, with two fields reaching a depth of $r_{AB} < 19.4$ mag and the third extending to $r_{AB} < 19.8$ mag, together with $K_{AB} < 17.6$ mag over all three fields. There are ∼120 000 galaxies with measured spectra available from GAMA observations to date (Driver et al. 2011). The redshift of each galaxy is determined using runz (Saunders, Cannon & Sutherland 2004), a FORTRAN program for measuring redshifts from reduced spectra.

2.2 Data

The standard strong optical emission lines are measured from each curvature-corrected and flux-calibrated spectrum assuming a single Gaussian approximation and common values for redshift and linewidth (Hopkins et al., in preparation). Corrections for the underlying stellar absorption, dust obscuration and fibre aperture effects, detailed below, are applied to these measurements. A full composite line and continuum extraction process are ultimately intended for the full data set.

The strength of Hα emission in galaxy spectra is used in this investigation to probe the extent of the star formation in galaxies. The Hα luminosity is used to measure the current SFR, as the ionizing photons mainly come from short-lived massive stars. Our sample is drawn from the ∼120 000 spectra available at 2010 June, and comprises 43 668 galaxies with measured emission lines, about 40 per cent of all galaxies in the GAMA sample at that time. This sample only includes objects with redshift quality flags ≥3 (i.e. regarded as a secure redshift; see Driver et al. 2011). Furthermore, we exclude all galaxies with Hα emission measurements affected by the presence of strong sky lines (see Fig. 2), and all galaxies with Hα emission below a minimum flux limit of $25 \times 10^{-17}\,\mathrm{erg\,s^{-1}\,cm^{-2}}$. This flux limit is obtained from examining the spectra of a sample of low Hα luminosity galaxies. Increasing this flux limit to that used by Brough et al. (2011) for a sample of low Hα luminosity GAMA galaxies, for example, does not alter our conclusions. Sloan Digital Sky Survey (SDSS) photometry in *u,g,r,i,z* filters is available for each galaxy (Hill et al. 2011). *k*-corrections to $z = 0.1$ are applied and all photometry is corrected for foreground (Milky Way) dust-extinction (Schlegel, Finkbeiner & Davis 1998; Blanton & Roweis 2007). The galaxy sample covers a moderate range in redshift ($0 < z \leq 0.35$). Galaxies dominated by emission from active galactic nuclei (AGN) are excluded from the sample (5334 galaxies) based on standard optical emission-line ([N II]/Hα and [O III]/Hβ) diagnostics using the discrimination line of Kewley et al. (2001). In the case of galaxies for which only some of these four emission lines are measurable, AGNs can still be excluded using the diagnostics log ([N II]/Hα) ≥ 0.2 and log ([O III]/Hβ) ≥ 1. This excludes a further 173 galaxies. The size of the final sample is 33 657.

This sample of galaxies spans a large range in stellar mass [$7 \leq \log(M/\mathrm{M}_{\odot}) \leq 12$] and SFR ($10^{-3}$ to 100 $\mathrm{M}_{\odot}\,\mathrm{yr}^{-1}$). It is this

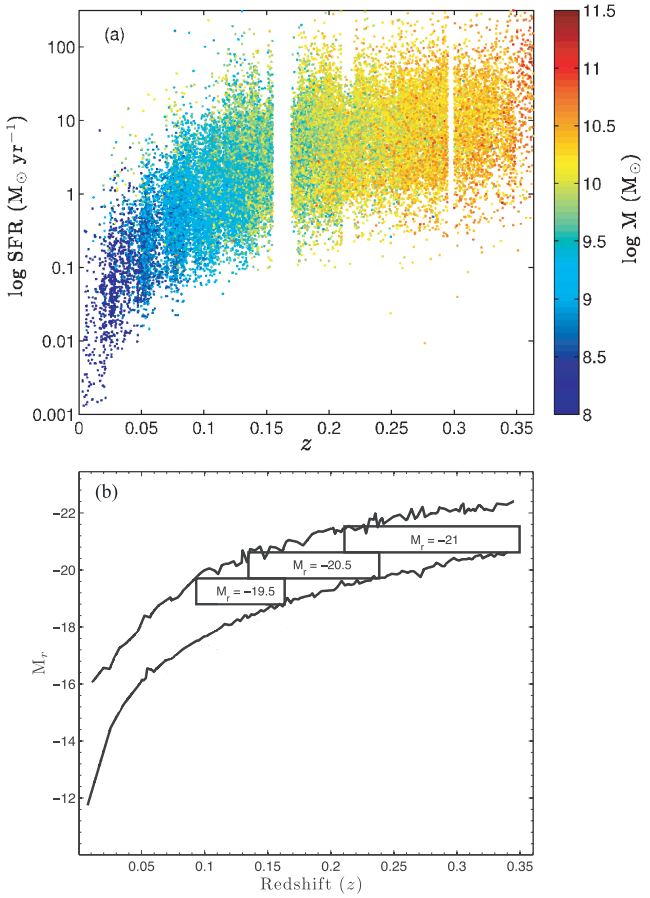

Figure 1. (a) The distribution of SFR and galaxy stellar masses with redshift. The visible gap in the distribution centred on $z = 0.16$ shows where the wavelength of the atmospheric O_2 band (Fraunhofer A-line) overlaps with the redshifted wavelength of the Hα emission line, leading us to omit these data from our analysis. The masses are in units of the solar mass, 1 $M_\odot$ = 1.99×10^{30} kg. (b) The definition of the volume-limited samples used in this study. The galaxies within each magnitude range are not affected by the flux limits of the survey, so that each of the three samples is complete to a given luminosity.

large range in SFR, stellar mass and redshift that permits us to explore the potential IMF dependencies with respect to different physical properties of galaxies. Fig. 1(a) shows the wide range in SFR sampled as a function of redshift, and colour coded to illustrate the range in stellar masses. Fig. 1(b) shows the envelope of the distribution of absolute *r*-band magnitude, M_r, with redshift for this sample. Outlined within this envelope are three independent volume-limited samples which form the basis of our subsequent analysis. These are selected to span ∼1 mag in M_r, centred on the values shown.

3 DERIVING PHYSICAL QUANTITIES

3.1 Hα luminosities

The observed Hα emission must be corrected for the effects of stellar absorption within the host galaxy, obscuration by dust and the limited sampling of each galaxy by the optical fibres (aperture effects) used in multi-object spectroscopy.

3.1.1 Stellar absorption correction and Balmer decrements

A simple constant correction for stellar absorption in Balmer emission-line equivalent widths (EWs) (i.e. Hα and Hβ EWs) is used for this investigation. The assumed common EW correction (EW_c) for the stellar absorption in the GAMA data is 1.3 Å. Based on previous work (Hopkins et al. 2003), a correction of at the most 1.3 Å is sufficient, provided the assumption is restricted to studies examining the gross characteristics of a large sample of sources, which is the case in this investigation. We tested a range of EW_c values between 0.7 and 1.3 Å, and the results did not vary measurably. Only Hα EWs smaller than log (Hα EW) < 0.9 show a difference in EW of more than 5 per cent.

As the stellar absorption may in general be a luminosity-dependent quantity, the required correction could be higher for high SFR sources. In order to test this aspect, a unique EW_c for each galaxy is assigned based on an assumed linear relationship between luminosity and stellar absorption correction. The results indicate that a luminosity-dependent stellar absorption correction does not significantly affect the calculated intrinsic luminosity of the source. Less than 10 per cent of the sample showed any noticeable effect. For systems with log (Hα EW) > 2, the assumption of a luminosity-dependent absorption correction increases the inferred EWs for these extreme systems, thereby further enhancing the trend with SFR presented in this paper. Therefore, the assumption of a fixed $EW_c = 1.3$ Å should not significantly affect the trends evident in the results, or our conclusions.

The Balmer Decrement (BD) is defined as the ratio of stellar absorption corrected Hα to Hβ fluxes (BD $= S_{H\alpha}/S_{H\beta}$), where $S_{H\alpha}$ for example is (Hopkins et al. 2003)

$$S_{H\alpha} = F_{H\alpha} \times \frac{(H\alpha EW + EW_c)}{H\alpha EW}, \quad (1)$$

where $F_{H\alpha}$ is the measured emission-line flux.

A small fraction of galaxies have BDs less than the Case B recombination value BD = 2.86 (Fig. 2). The BD is an obscuration-sensitive parameter, and its departure from the Case B recombination value of 2.86 is an indication of the dust attenuation along the line of sight. BD < 2.86 can result not only from an intrinsically low reddening combined with uncertainty in the stellar absorption, but also from errors in the line flux calibration and measurements (Kewley et al. 2006). Out of all the galaxies with measured BDs, ∼6 per cent have BD < 2.86. All these BDs are set to 2.86 for the purpose of this investigation.

Not all galaxies have both Hα and Hβ measurements. For the galaxies with only Hα measurements, the relation between aperture-corrected luminosity and BD is used to determine the BDs. The empirical form of the relationship between aperture-corrected luminosity and BD is shown in Fig. 2. The form is

$$\begin{aligned} BD &= 0.81 \log(L_{H\alpha,ACor}) - 22.041, \quad \log(L_{H\alpha,ACor}) > 30.74 \\ &= 2.86, \quad \log(L_{H\alpha,ACor}) \leq 30.74, \end{aligned} \quad (2)$$

where $\log(L_{H\alpha,ACor})$ denotes the aperture-corrected Hα luminosity (see equation 3).

3.1.2 Aperture correction

Aperture effects arise from the physical limitation imposed by the diameter of the spectroscopic fibre used in the observations. For nearby sources, this means that the fibre only captures part of the light from the object, which is naturally a problem for sources larger in size than the fibre diameter projected on the sky. An

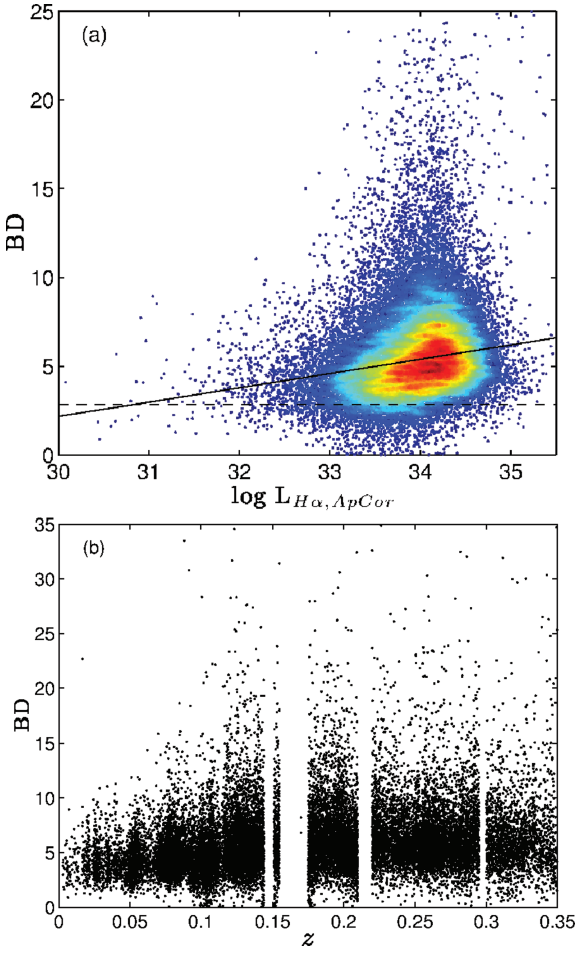

Figure 2. (a) The relationship between BDs and aperture-corrected luminosities for the galaxies with accurate Hα and Hβ EW measurements. A linear relation is fitted to the data to determine the BDs for the galaxies that have measured Hα EWs but no Hβ EWs or have Hβ EWs that are affected by sky absorption bands. (b) The dust obscuration as indicated by the BD is the largest at high z. This is because high SFR objects also tend to have higher obscurations (Hopkins et al. 2001) and the objects at higher z tend to have higher SFRs, a result of both galaxy evolution and a predominance of massive, high-SFR galaxies at high z, due to the flux limit of the survey.

aperture correction is required to account for the missing flux, in order to get an estimate of the true SFR. Following the approach used for SDSS spectra by Hopkins et al. (2003), we implemented an aperture correction for the Hα luminosities of the GAMA galaxies. This approach uses the absolute r-band magnitude to approximate the continuum at the wavelength of Hα, thereby accounting for the Hα luminosity of the whole galaxy (equation 3). Fig. 3 shows the relation between the applied aperture correction and z and the required correction is typically a factor of 2–4.

The aperture-corrected Hα luminosity ($L_{\rm H\alpha,ACor}$) for the whole galaxy is a function of three parameters, Hα EW (EW$_{\rm H\alpha,obs}$), absolute r-band luminosity (M_r) and redshift (z). The form of the aperture-corrected luminosity before applying any obscuration correction is (Hopkins et al. 2003)

$$L_{\rm H\alpha,ApCor} = ({\rm EW}_{\rm H\alpha,obs} + {\rm EW}_{\rm c}) \times 10^{-0.4(M_r-34.10)} \times \frac{3\times10^{18}}{(6564.61(1+z))^2}. \quad (3)$$

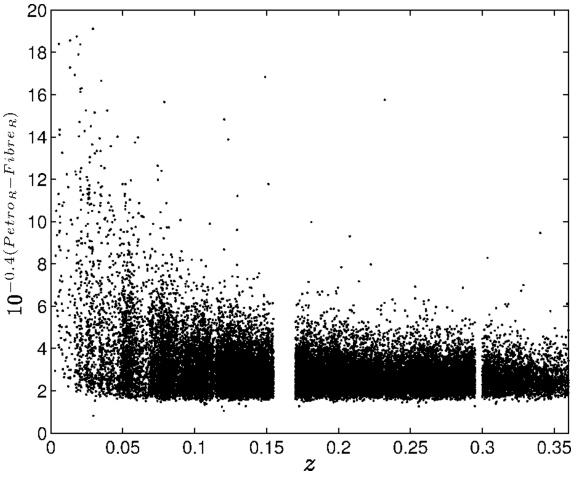

Figure 3. Aperture correction factor as a function of redshift. The required aperture correction is the largest at low z because low z objects are more likely to be larger in angular size than the aperture of the spectroscopic fibre used for the observations.

The aperture corrections are based on the absolute magnitude, M_r, of each galaxy as an estimate of continuum luminosity, thereby recovering an Hα luminosity for the whole galaxy. This method of applying aperture corrections to the luminosities, described in Hopkins et al. (2003), yields similar results to the more complex colour gradient based aperture corrections described in Brinchmann et al. (2004). We use these aperture-corrected values throughout this analysis. We have, in addition, tested the effect on our results in the case of using SFRs estimated only from the detected Hα emission through the fibre (no aperture corrections). Even in this case, we find the same qualitative conclusions regarding the SFR-dependence of IMF slope. We conclude that the aperture corrections applied here are not introducing any significant bias, nor are they erroneously giving rise to our results.

The aperture, obscuration and stellar absorption corrected luminosity for the whole galaxy is given as

$$L_{\rm H\alpha,int} = ({\rm EW}_{\rm H\alpha} + {\rm EW}_{\rm c}) \times 10^{-0.4(M_r-34.10)} \times \frac{3\times10^{18}}{(6564.61(1+z))^2}\left(\frac{F_{\rm H\alpha}/F_{\rm H\beta}}{2.86}\right)^{2.36}, \quad (4)$$

where $F_{\rm H\alpha}/F_{\rm H\beta}$ denotes the BD. Fig. 2(b) explores the increase in BD with respect to increasing z. The exponent of the BD in equation (4) is equal to $k(\lambda_{\rm H\alpha})/[k(\lambda_{\rm H\beta}) - k(\lambda_{\rm H\alpha})]$, where extinction at a given λ, $k(\lambda)$, is determined from the Cardelli, Clayton & Mathis (1989) galactic dust obscuration curve.

The Hα SFR can be determined from Kennicutt (1998)

$${\rm SFR}_{H\alpha} = \frac{L_{\rm H\alpha}}{1.27\times10^{34}}. \quad (5)$$

The derivation of the Hα SFR calibration requires the assumption of an IMF. The above calibration factor has been derived assuming a Salpeter IMF. Table 1 shows the effect on the SFR calibrator if a different IMF is assumed. For a given luminosity, a calibration based on a flatter IMF would indicate a lower SFR than the Salpeter IMF-based calibration.

If an IMF-dependent SFR calibration is used in the derivation of SFRs for GAMA galaxies, that would reduce the range in SFR shown in Fig. 1(a). This reduction in range would not affect our main conclusion of an IMF–SFR relationship, because the SFR

Table 1. The SFR calibration factors for different IMFs.

High-mass slope	Calibration factor (W)
$\alpha = -2.00$	4.08×10^{34}
$\alpha = -2.35$	1.27×10^{34}
$\alpha = -2.50$	0.65×10^{34}

calculated for the sample would still vary monotonically (as the scaling is linear, the ordering of the SFRs is not affected).

3.2 The determination of stellar masses

The stellar masses used in this investigation are derived based on the observed tight relation between $(g - i)$ colour and the mass–luminosity (M/L) relation (Taylor et al. 2010) using the Bruzual & Charlot (2003) models and assuming a Chabrier (2003a) IMF. This method of calculating the masses yields results consistent with other established techniques (e.g. Baldry et al. 2006).

$$\log(M_*) = -0.68 + 0.73(g - i) - 0.4(M_i - M_{i,\odot}), \quad (6)$$

where M_* is the mass of the galaxy, g and i band colours are k-corrected to $z = 0$, M_i is the absolute magnitude of the galaxy in the i band and $M_{i,\odot} = 4.58$, the absolute magnitude of the Sun in the i band.

4 OBSCURATION CORRECTIONS

Understanding and interpreting the physical and chemical properties of galaxies depend in part on how accurately the data are corrected for stellar absorption and dust obscuration to recover the intrinsic fluxes. Hα can be heavily attenuated by dust. High SFR galaxies are subjected to greater dust obscuration than lower luminosity objects (Hopkins et al. 2001, 2003; Afonso et al. 2003; Pérez-González et al. 2003). Obscuration corrections are especially critical in this analysis as our primary aim is to compare the observed Hα EW and $g - r$ (or $g - i$) colours with PÉGASE generated synthetic spectra for different input IMFs, assuming no extinction.

The reliability of the applied dust correction depends on the adopted dust obscuration models. We explore several popular empirical dust models (Cardelli et al. 1989; Calzetti 2001; Fischera & Dopita 2005) along with radiative transfer model predictions of the effects of dust extinction (Popescu et al. 2000; Tuffs et al. 2004; Popescu et al. 2011).

The differential reddening between the stellar continuum and gas (Calzetti 2001) must be addressed in deriving the intrinsic fluxes. The difference in attenuation between gas and continuum is generally assumed to be ∼2 (Calzetti 2001; Hoversten & Glazebrook 2008; Meurer et al. 2009; Wijesinghe et al. 2011). Hoversten & Glazebrook (2008) describe the effect, on Hα EWs and colours, of varying the differential reddening factor between the continuum and gas. We tested the impact of this assumption on our results. For all the subsequent analysis in this paper we use obscuration-corrected colours derived through the application of an obscuration curve together with this factor of ∼2 (as detailed below). These measurements were compared against colours derived by Taylor et al. (2011), from full SED modelling of the GAMA photometry, with independent dust corrections. The results are consistent, with an rms scatter of ∼0.17 mag, with no systematic deviation, as might be expected if the factor of ∼2 between gas and continuum obscuration were significantly in error. There is, moreover, no systematic offset in these two approaches as a function of SFR, specific SFR, mass or redshift. We conclude that our assumption of this commonly used factor is justified, and unlikely to introduce any systematic error in our result.

The obscuration-corrected Hα EW is given as

$$\mathrm{EW}_{\mathrm{H}\alpha,\mathrm{int}} = \frac{(\mathrm{EW}_{\mathrm{H}\alpha,\mathrm{obs}} + 1.3)}{(1+z)} \times 10^{0.4[k(\lambda_{\mathrm{H}\alpha})E(B-V)_{\mathrm{gas}} - k(\lambda_{\mathrm{H}\alpha})E(B-V)_*]}, \quad (7)$$

where $k(\lambda)$ gives the extinction at wavelength λ, and the colour excess of gas (i.e. emission lines) is

$$E(B-V)_{gas} = \frac{\log\left(\frac{\mathrm{H}\alpha}{\mathrm{H}\beta}/2.86\right)}{0.4[k(\lambda_{\mathrm{H}\beta}) - k(\lambda_{\mathrm{H}\alpha})]}. \quad (8)$$

The colour excess of the continuum (Calzetti 1997) is

$$E(B-V)_* = 0.44E(B-V)_{\mathrm{gas}}. \quad (9)$$

The effect of the spectroscopic fibre sampling only the central regions, for those galaxies largest on the sky, may be to limit the detection of the lowest EW systems in low SFR galaxies. Accounting for this effect would not change our results; indeed, if anything, such a correction would act to enhance the trend investigated here.

4.1 Applying obscuration corrections

This section describes the different obscuration curves used in this analysis, and the methods of applying obscuration corrections to the data.

We have used a combination of the Calzetti (2001) and Cardelli et al. (1989) obscuration curves and the Fischera & Dopita (2005) curve as described by Wijesinghe et al. (2011) to determine the necessary corrections. These extinction curves and the application of dust corrections are described below.

4.1.1 Calzetti (2001) obscuration law

This dust extinction curve is appropriate for continuum attenuation corrections as this curve is derived from spatially integrated colours of the entire stellar population in a sample of starburst galaxies. Embedded within the analytical form of this curve are dust geometry and composition, and it mostly describes dust absorption, since the effects due to scattering are averaged out. Because the entire stellar population within the galaxies was observed, emission lost through dust scattering out of the line of sight is averaged out by the scattering into the line of sight. The form of the curve is

$$\begin{aligned} k(\lambda) &= 2.656\left(-1.857 + \frac{1.040}{\lambda}\right) + 4.05, \\ &\quad \text{for } 0.63\,\mu\mathrm{m} \le \lambda \le 2.2\,\mu\mathrm{m} \\ &= 2.656\left(-2.156 + \frac{1.509}{\lambda} - \frac{0.198}{\lambda^2} + \frac{0.011}{\lambda^3}\right) + 4.05, \\ &\quad \text{for } 0.12\,\mu\mathrm{m} \le \lambda < 0.63\,\mu\mathrm{m}. \end{aligned} \quad (10)$$

The second term of the exponent in equation (7), which is related to the continuum luminosity, and the corrections to the colours are derived using this curve.

4.1.2 Cardelli et al. (1989) obscuration law

This Galactic dust obscuration curve is derived from observations of the UV extinction of stars, as well as using various other sources for optical and NIR data. The young stellar populations in massive star-forming regions responsible for UV radiation are also responsible for nebular emission lines and this curve is applicable to both diffuse and dense stellar regions. This curve accurately describes the dust effects on emission lines and has the form

$$k(\lambda) = a(x) + \frac{b(x)}{R_v}, \tag{11}$$

where R_v is the ratio of total to selective extinction and is a constant for a given extinction curve. The value of $R_v = 3.1$ (Calzetti 2001), which is found to well describe the reddening of the ionized gas in star-forming galaxies, is used in this analysis.

The functional forms of $a(x)$ and $b(x)$ in equation (11), with $x = 1/\lambda$, are a power law in the infrared regime and a polynomial in the optical/NIR regime, in units of μm^{-1}:

Infrared: $0.3\,\mu m^{-1} \leq x \leq 1.1\,\mu m^{-1}$;

$$a(x) = 0.574\lambda^{1.61};$$

$$b(x) = -0.527\lambda^{1.61}.$$

Optical/NIR: $1.1\,\mu m^{-1} \leq x \leq 3.3\,\mu m^{-1}$ and $y = (x - 1.82)$;

$$a(x) = 1 + 0.17699y - 0.50447y^2 - 0.02427y^3 + 0.72085y^4 + 0.01979y^5 - 0.7753y^6 + 0.32999y^7;$$

$$b(x) = 1.41338y + 2.28305y^2 + 1.07233y^3 - 5.38434y^4 - 0.62251y^5 + 5.30260y^6 - 2.09002y^7. \tag{12}$$

The first term of the exponent in equation (7) related to the line luminosity is based on this curve. The intrinsic Hα EW is the ratio of the corrected Hα line to continuum luminosities.

4.1.3 Fischera & Dopita (2005) obscuration law

A recent study by Wijesinghe et al. (2011), looking at dust obscuration in galaxies using GAMA data, tested a number of common obscuration curves, including the Calzetti (2001, 1997), and Cardelli et al. (1989) dust curves. They found that a Fischera & Dopita (2005) obscuration curve with $R_v = 4.5$ and the 2200Å bump removed gives an excellent agreement between far-ultraviolet, near ultraviolet, Hα and [O II] derived SFR indicators.

In this case, both terms of the exponent in equation (7) and the corrections to the colours are determined using the Fischera & Dopita (2005) curve.

4.2 Popescu et al. (2000, 2011) and Tuffs et al. (2004) radiative transfer models

In addition to the dust corrections based on the above dust obscuration curves, the effects of dust attenuation on Hα EW and $g - r$ parameters can be determined using radiative transfer models (Popescu et al. 2000; Tuffs et al. 2004; Popescu et al. 2011), where the attenuation of star light from disc galaxies with different dust geometries of different stellar ages constrained by UV/optical to FIR/submm spectral energy distributions is considered. The model predictions are based on the opacity of the diffuse dust component, given as face-on B-band optical depth (τ_b), inclination of a galaxy and a clumpiness factor (F) describing the local absorption of UV light from massive stars due to the presence of massive star-forming regions.

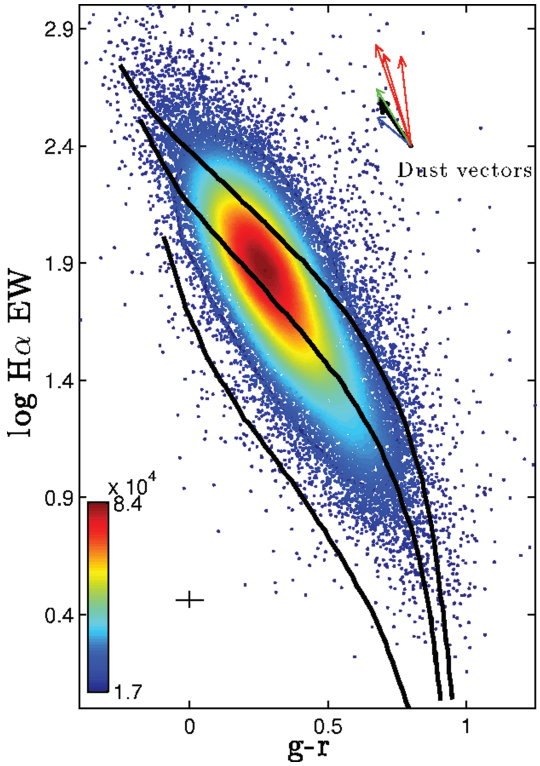

Figure 4. Distribution of all GAMA galaxies up to $z = 0.355$, after dust corrections as given in the text. All data and the model tracks are k-corrected to $z = 0.1$. The colour contours indicate the data density and the three solid lines indicate the three different evolutionary paths a galaxy would take if all star clusters within that galaxy have an IMF with a slope of $\alpha = -3$ (bottom track), $\alpha = -2.35$ (middle track) or $\alpha = -2$ (top track). These model tracks are generated using PÉGASE. The arrows depict the dust vectors. The red arrows represent radiative transfer model predictions calculated using the model of Popescu et al. (2000, 2011) and Tuffs et al. (2004) and from left to right correspond to $\tau_b = 8, 4, 1$, all assuming a median galaxy inclination of 60° and $F = 0.35$. The rest of the vectors show the movement of data points for different dust extinction curves and for a BD of 4. Blue: the dust vector calculated using the Calzetti (1997) curve for the continuum corrections and Cardelli et al. (1989) curve for emission-line corrections. Green: the dust vector corresponding to corrections calculated using Fischera & Dopita (2005) curve as modified by Wijesinghe et al. (2011). Black: the dust vector corresponding to the Calzetti (2001) and Cardelli et al. (1989) curves for the continuum and emission corrections, respectively.

These various approaches to obscuration corrections are detailed as vectors in Fig. 4, showing the effect of different obscuration curves, or models, on the data, for an assumed Balmer decrement of $BD = 4$. As shown in more detail below, the different approaches to dust correction do not change our qualitative conclusions.

5 EVIDENCE FOR A NON-UNIVERSAL IMF

The three model evolutionary tracks shown as black lines in Fig. 5 are reproduced from Hoversten & Glazebrook (2008). These evolutionary tracks are generated using the population synthesis code PÉGASE (Fioc & Rocca-Volmerange 1997), under the assumption of no extinction and an exponentially declining star formation history with an e-folding time of 1.1 Gyr. The model evolutionary tracks denoted by the red lines are generated by combining Maraston (2005) and PÉGASE models. Based on a similar analysis of Hα EW and $g - r$ colour, Hoversten & Glazebrook (2008) suggest a possible

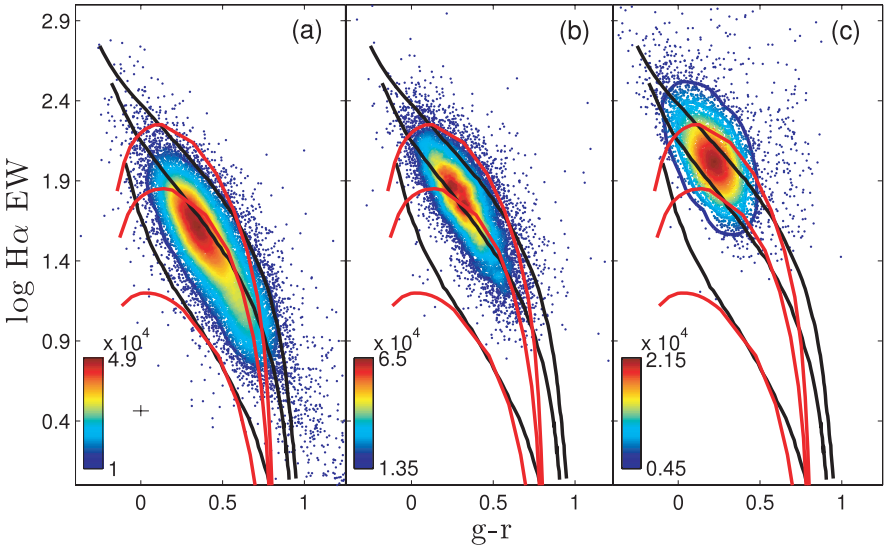

Figure 5. The sample of GAMA galaxies divided into three sub-samples based on SFRs. (a) $0 < \mathrm{SFR}\,(\mathrm{M}_\odot\,\mathrm{yr}^{-1}) < 3$, (b) $3 \leq \mathrm{SFR}\,(\mathrm{M}_\odot\,\mathrm{yr}^{-1}) < 13$ and (c) $\mathrm{SFR}\,(\mathrm{M}_\odot\,\mathrm{yr}^{-1}) \geq 13$. The two sets (black and red) of three solid lines indicate the three different evolutionary paths a galaxy would take in Hα EW and $g - r$ colour if all star clusters within that galaxy have an IMF with a slope of $\alpha = -3$ (bottom track), $\alpha = -2.35$ (middle track) or $\alpha = -2$ (top track). The black lines are the evolutionary paths predicted by PÉGASE (Fioc & Rocca-Volmerange 1997) and red lines are paths predicted by Maraston (2005) models. The age increases along the tracks from 100 Myr (top left) to 13 Gyr (bottom right). Coloured contours are drawn based on data densities of each sub-sample. The ranges in data densities are indicated alongside the colour bars of each plot. A representative uncertainty on individual measurements is indicated by the error bars in the bottom left of (a). A variation with SFR is apparent across the three panels, with high star-forming sources evidently preferring a flatter IMF.

systematic variation in the IMF slope, in which faint galaxies prefer steep IMFs. Our results (Fig. 5), shown for three sub-samples based on SFR, are consistent with those of Hoversten & Glazebrook (2008), and are not sensitive to the choice of population synthesis models. The low-luminosity systems, which also have low SFRs (Fig. 5a), lie below the central model track representative of a Salpeter IMF ($\alpha = -2.35$) and towards the bottom track with $\alpha = -3$. In contrast, those with high SFRs lie towards the top model track with $\alpha = -2$.

A clear variation in IMF slope with the SFR of the host galaxy is evident in Fig. 5, where the high SFR systems are characterized by a flatter IMF. In order to quantify this effect, the same analysis is performed using three independent volume limited samples, with absolute r-band magnitude ranges centred on $M_r = -21$, 20.5 and -19.5 shown in Fig. 1(b), where each sample is complete to a given r-band luminosity. This avoids the bias against lower SFR systems at higher redshifts, imposed by our optical/near-infrared magnitude and Hα flux-limited selection. Each sample is further divided into eight sub-samples based on SFR (Fig. 6). The clear progression towards a top-heavy, or flatter, IMF with increasing SFR is evident in all three independent volume-limited samples.

The general trend measured here is that low SFR galaxies populate the lower right of the Hα EW and colour plane, being characterized by Salpeter, or steeper, IMF slopes. With increasing SFR, the galaxy population moves upwards to the left from a steep to a flat IMF track, implying a SFR dependence of the high-mass IMF slope. Given the low-redshift range ($0 < z \leq 0.35$) of the sample, the observed IMF–SFR effect cannot be a result of merging systems since the merger rate is very low, $\sim$2 per cent (De Propris et al. 2007; Lotz et al. 2008) at these low redshifts, and the high-SFR systems are not dominated by mergers.

5.1 The effect of dust extinction

Fig. 7 compares the uncorrected results with dust obscuration corrected using the Cardelli et al. (1989) and Calzetti (2001) obscuration curve combination and the Fischera & Dopita (2005) obscuration curve as given by Wijesinghe et al. (2011).

The effect of dust from each of the prescriptions investigated is to move data points parallel to the model evolutionary tracks. The progression of data orthogonal to the tracks, as SFR varies, is unlikely to be a consequence of erroneous dust obscuration corrections. Finally, increasing τ_b does not affect Hα EW except at high inclinations, where Hα is attenuated more than the r band due to the low scaleheight. Therefore, if there is an increase in disc opacity (τ_b) as a function of SFR, this effect would not cause a systematic shift of data points orthogonal to the model tracks, mimicking the trend with SFR presented in this paper. Any such effect due to the presence of dust causes the raw data points to move downwards parallel to the model tracks.

5.2 Addressing the systematics

Here we explore how the modification of the other free parameters of the population synthesis models, as well as the introduction of additional models, affects our results.

5.2.1 Effects of modifying the free parameters

The three model evolutionary tracks plotted in previous figures and shown as dashed lines in Fig. 8 are generated assuming an exponentially decreasing star formation history with e-folding time of 1.1 Gyr, $Z = 0.02$ (solar metallicity) and an upper stellar mass limit of 120 $\mathrm{M}_\odot$ for different input IMFs. Fig. 8 explores the effects

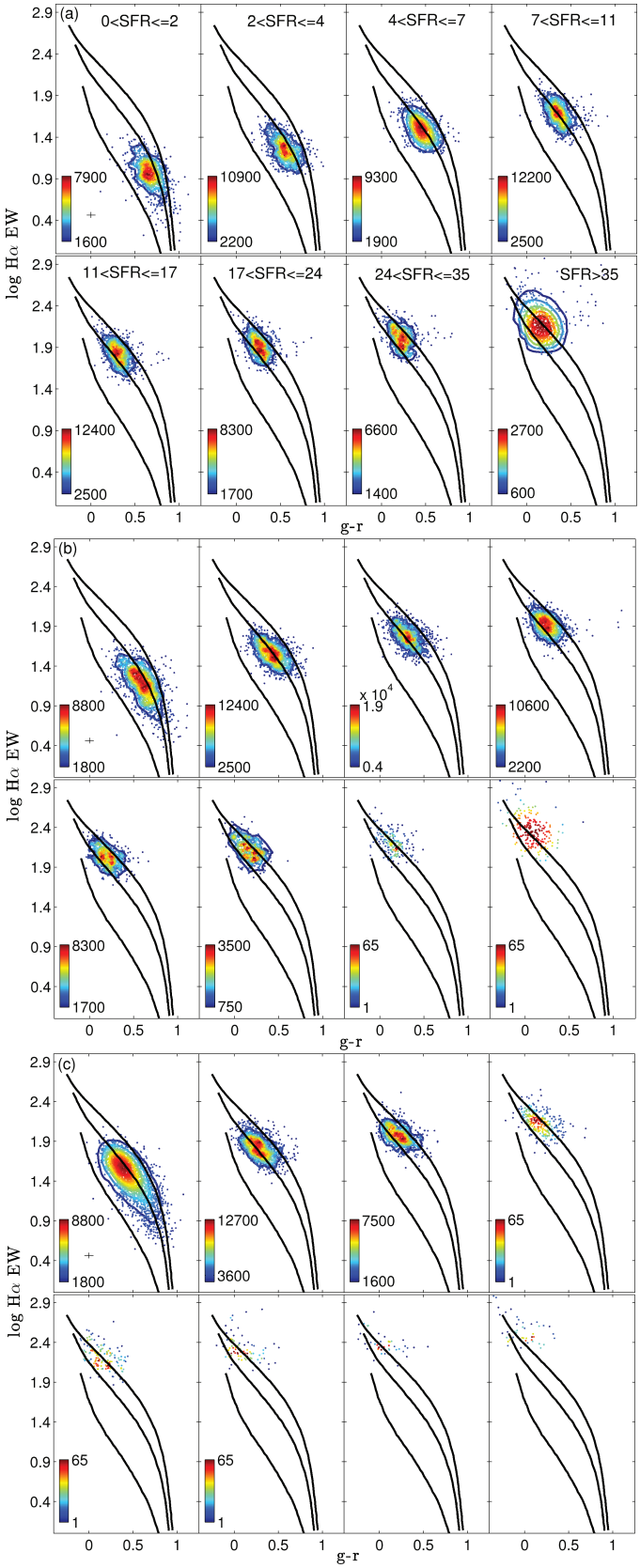

Figure 6. Three independent volume-limited samples $\langle M_r, z\rangle = -21, 0.29$ (a), $\langle M_r, z\rangle = -20.5, 0.19$ (b) and $\langle M_r, z\rangle = -19.5, 0.13$ (c) divided into eight SFR sub-samples. A representative uncertainty on individual measurements is indicated by the error bars in each top-left panel. The IMF–SFR relationship is evident in each independent volume-limited sample. The coloured contours are based on the data densities and the ranges of these densities are indicated alongside each colour bar.